Front. Optoelectron. 2019, 12(3): 268–275
https://doi.org/10.1007/s12200-019-0848-y

RESEARCH ARTICLE

Optimization of organic light emitting diode for HAT-CN based nano-structured device by study of injection characteristics at anode/organic interface

Neha JAIN[1], O. P. SINHA[2], Sujata PANDEY (✉)[3]

1 Department of Electronics and Communication Engineering, Amity University UP, Noida, India
2 Amity Institute of Nanotechnology, Amity University UP, Noida, India
3 Department of Electronics and Telecom Engineering, Amity University UP, Noida, India

Abstract To increase the current density of the hole only device, 1, 4, 5, 8, 9, 11-hexaazatriphenylene-hexacarbonitrile (HAT-CN) material has been inserted in the device at the indium tin oxide (ITO)/organic interface. Since HAT-CN molecule can withdraw electrons, it can alter electronic properties of the electrodes and hence inserted between the organic/metal interfaces. This paper deals with the optimization of the thickness of organic-metal layers to enhance the efficiency. Also, efforts have been made to increase the current density and reduce the operating voltage of the device. The material 2, 7-bis [*N*, *N*-bis (4-methoxy-phenyl) amino]-9, 9-spirobifluorene (Meo-Spiro-TPD) is used to simulate the hole only device because it is a thermally stable hole transport material. Simulated results shows that better current density values can be achieved compared to fabricated one by optimizing the organic metal layer thickness. The best optimized layer thickness of 22 nm for Alq_3, 25 nm for CBP* doped with $Ir(ppy)_3$, 9 nm for Meo-Spiro TPD and 4 nm for HAT-CN which results in current density of 0.12 A/cm^2 with a reduction in operating voltage by approximately 2 V.

Keywords organic light emitting diode (OLED), 2, 7-bis [*N,N*-bis (4-methoxy-phenyl) amino]-9, 9-spirobifluorene (Meo-Spiro-TPD), indium tin oxide (ITO), model, higher occupied molecular orbital (HOMO), lower unoccupied molecular orbital (LUMO)

Received July 3, 2018; accepted August 30, 2018

E-mail: spandey@amity.edu

1 Introduction

Organic light emitting diodes (OLEDs) are very popular these days due to its application in solid state lighting and for display devices. Due to excellent characteristics of OLEDs like very less power consumption, high brightness and flexibility, OLEDs are considered as a very superior source of solid state lightning. OLEDs also have a very wide range of applications like they are used in mobile gadgets, television screen, computer monitors, car lighting, and games consoles etc. OLEDs generally composed of stacked layers of electrode/organics/electrode. Among these two electrodes, at least one of them is transparent [1–16].

The energy level of higher occupied molecular orbital (HOMO) and lower unoccupied molecular orbital (LUMO) alignment plays a very important role in the study of the charge transport and injection mechanism. This is because organic semiconductors have negligible doping concentration and have very less charge density [3]. Due to this reason, electrodes are responsible for injecting all charges in OLED devices. In this paper, the theoretical model for recombination is presented and discussed. Also, the effect of applied voltage on recombination is investigated in stacked nano-structured organic light emitting diode [5]. To enhance the current density, distribution can be solved by taking in to consideration of drift diffusion equations [6]. These equations are based on Langevin recombination rate. Also, the Poole Frenkel model depends on electric field for the calculation of carrier mobility of the device to be simulated [6]. To enhance the device performance, vast understanding and knowledge of the physical phenomena and methodology is

* 4,4′-bis(*N*-carbazolyl)-1,1′-biphenyl (CBP), iridium, tris[2-(2-pyridinyl-κN)phenyl-κC] ($Ir(ppy)_3$)

needed regarding the transport and injection characteristics of charge carriers. Lee et al. reported in Ref. [17] that the properties and thickness of the electron transport layer (ETL) can be crucial for the achievement of improved charge balance. Also, ETL is also responsible for the recombination zone detention in phosphorescent OLED to enhance device performances. Also the refractive index of ETL is a factor to enhance the performance. It has been observed that lower the refractive index; higher will be the performance of the device [18]. Position and orientation of the molecules of emitter strongly influence the efficiency roll-off in OLEDs. This can be investigated by changing the distance between the emitter and metal cathode. Molecular doping of organic semiconductors is also an important step in enhancing the performance of an OLED. A lot of work has been done on the doped transport layer applications. This is due to the fact that the conductivity of organic materials can be enhanced by doping with acceptor or donor atoms. In phosphorescent organic materials, the emitting layer (EML) is doped with another material such as Bis[2-(4,6-difluorophenyl)pyridinato-C2,*N*](picolinato) iridium(III) (FIrpic), fac-Tris(2-phenylpyridine)iridium ($Ir(ppy)_3$) etc. This is done to form a host-guest system to improve the quantum efficiency. In the present work, $Ir(ppy)_3$ is used as the guest material for doping of CBP. This depends on the selection of doping material as already discussed about CBP-$Ir(ppy)_3$ host-guest materials. In the present work, electron acceptor dopants like HAT-CN are used to the doped hole transporting layers [2–4,13,19].

Recently our group has published the experimental results with structure shown in Ref. [2]. Taking this experimental data, we simulated the OLED for different layer parameters and found the best optimised conditions for efficient OLED. For this attainment, a stacked structure consists of 1, 4, 5, 8, 9, 11-hexaazatriphenylene-hexacarbonitrile (HAT-CN), 2, 7-bis [*N*, *N*-bis (4-methoxy-phenyl) amino]-9, 9-spirobifluorene (Meo-Spiro-TPD), 4,4'-*N*,*N* dicarbazolylbiphenyl (CBP) doped with $Ir(ppy)_3$ and tris (8-hydroxyquinolinato)aluminum(III) (Alq_3). HAT-CN and Meo-Spiro-TPD have certain advantages as hole injection layer (HIL) and hole transport layer (HTL) respectively which enhances the hole transport efficiency of p-type materials. Meo-TPD can be used as HTL because it has high range of glass transition temperature [10,11,14].

2 Device structure and input parameters for simulation

In the present work, simulated OLED consists of stacked structure of HAT-CN, Meo-Spiro-TPD, $Ir(ppy)_3$ doped CBP and Alq_3 with electrodes aluminum (Al)/lithium flouride (LiF) and indium tin oxide (ITO). Here Al/LiF acts as anode and ITO act as cathode. Current density versus voltage (*J-V*) measurement was performed using the Silvaco Atlas software. The active area of the devices is 2 mm × 2 mm. Current density values have been found by optimizing different layer thicknesses used in the structure shown in Fig. 1. Optimization results will be discussed in Section 3.

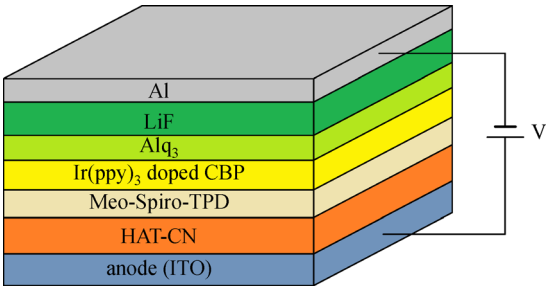

Fig. 1 Structure of simulated OLED

Figure 2 shows the energy band diagram for structure shown in Fig. 1. Rajan et al. in Ref. [2] reported electronic energy level of HAT-CN as LUMO = –5.42 eV and HOMO = –9.62 eV. Also, the Meo-Spiro-TPD energy levels have been reported [2] as LUMO = – 2.33 eV and HOMO = – 5.21 eV. In this OLED structure, HAT-CN layer is inserted between ITO and Meo-Spiro TPD interface. This is done to reduce the band gap between electrode and organic semiconductor interface. When a thin layer of HAT-CN is inserted, it acts as a virtual electrode which modifies the work-function of the substrate up to approx. 5.4 eV. This is due to the configuration of dipoles at these two interfaces. Work-functions of ITO and LiF/Al and HOMO-LUMO levels are also indicated in Fig. 2 [2].

For structure shown in Fig. 1, varying thicknesses of HAT-CN were used as HIL in between anode and organic layer interfaces. Similarly, different thicknesses for (Meo-Spiro-TPD), $Ir(ppy)_3$ doped CBP and Alq_3 were deposited for the better optimization of *I-V* and *J-V* characteristics.

3 Simulation and mathematical model

Traditionally, some models like Hoesterey-Letson formalism (HLF) and effective medium approximation (EMA) theory discussed the charge transport in organic materials (with traps). In this paper, Richardson thermionic model (RTM) is used. There is a formation of band-trap-band leakage path in the device at the metal/organic interface by the electron and hole emission traps. RTM has certain advantages, such as it provides main emission characteristics like beginning temperature of emission and also includes equations for emission from negative (or low) electron affinity (EA) materials. In addition, this model provides relationship between Richardson constant, EA and work-function of materials [2,20,21].

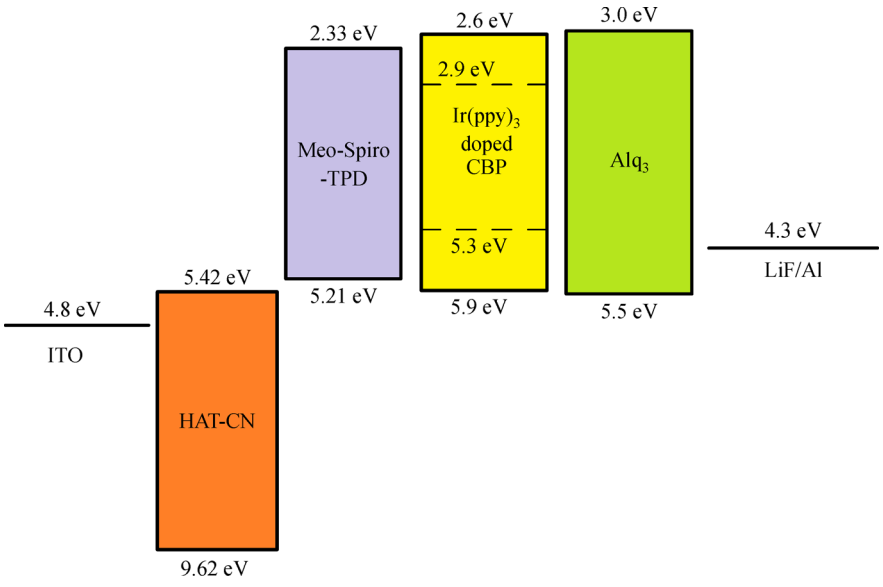

Fig. 2 HOMO-LUMO energy level diagram

3.1 Richardson thermionic model

In Richardson thermionic emission model, charge carriers gain required heat energy to rise above the band-gap at the interfaces. Therefore, the current density J is dependent on the temperature as well as electric field as given by Eq. (1) [2]:

$$J = AT^2 \exp\left\{\frac{-(\phi_b - \beta\sqrt{F})}{K_b T}\right\}, \tag{1}$$

where A is the field independent Richardson constant, given by [2,9]

$$A_n^* = \frac{4\prod qK^2 m_n^*}{h^3}, \tag{2}$$

$$A_p^* = \frac{4\prod qK^2 m_p^*}{h^3}. \tag{3}$$

where A_n^* is the field independent Richardson constant for electrons, A_p^* is the field independent Richardson constant for holes, m_n^* and m_p^* are the electron and hole effective masses.

ϕ_b is known as the zero-field injection barrier, K_b is the Boltmann constant and F is known as the electric field given by

$$F = V/d. \tag{4}$$

β is given by

$$\beta = \sqrt{\frac{q^3}{4\Pi\varepsilon\varepsilon_o}}. \tag{5}$$

where ε is the absolute permittivity and ε_0 is the electric permittivity of free space.

Finite surface recombination velocities can also be calculated using Eqs. (6) and (7) where V_{SURFN} is the actual surface recombination velocities for electrons and V_{SURFP} is the actual surface recombination velocities for holes,

$$V_{SURFN} = \frac{ARICHN \cdot T_L^2}{qN_c}, \tag{6}$$

$$V_{SURFP} = \frac{ARICHP \cdot T_L^2}{qN_v}. \tag{7}$$

Here, ARICHN is the effective Richardson constant for electrons and ARICHP is the effective Richardson constant for holes. Quantum mechanical reflections are considered for this calculation.

N_c and N_v are the conduction and valence band density of states and can be given by

$$N_c = 2\left(\frac{2\Pi m_e^* kT_L}{h^2}\right)^{\frac{3}{2}}, \tag{8}$$

$$N_v = 2\left(\frac{2\Pi m_h^* kT_L}{h^2}\right)^{\frac{3}{2}}. \tag{9}$$

3.2 Poole-Frenkel mobility model

The mobility equation is followed from the Poole-Frenkel model and its dependence on the electric field is given by the following equation [3]:

$$\mu_{eff} = \mu_0 \exp\left(-\frac{E_a - \sqrt{\beta F}}{kT}\right). \tag{10}$$

The Poole-Frenkel model can be explained by the following equations [8]:

$$\mu_{n\mathrm{PF}}(E) = \mu_{n0}\exp\left(\frac{\mathrm{DELTAEN.PFMOB}}{kT_{n_{\mathrm{eff}}}} + \left(\frac{\mathrm{BETAN.PFMOB}}{kT_{n_{\mathrm{eff}}}} - \mathrm{GAMMAN.PFMOB}\right)\sqrt{|E|}\right), \tag{11}$$

$$\mu_{p\mathrm{PF}}(E) = \mu_{p0}\exp\left(\frac{\mathrm{DELTAEP.PFMOB}}{kT_{p_{\mathrm{eff}}}} + \left(\frac{\mathrm{BETAP.PFMOB}}{kT_{p_{\mathrm{eff}}}} - \mathrm{GAMMAP.PFMOB}\right)\sqrt{|E|}\right), \tag{12}$$

where $\mu_{n\mathrm{PF}}(E)$ is the Poole-Frenkel mobility for hole and $\mu_{p\mathrm{PF}}(E)$ is the Poole-Frenkel mobility for electrons, μ_{n0} is the zero field mobility for electrons and μ_{p0} is the zero field mobility for holes, E is the electric field. DELTAEN. PFMOB and DELTAEP.PFMOB are the activation energies at zero electric field. $T_{p\mathrm{eff}}$ and $T_{n\mathrm{eff}}$ are the effective temperature for holes and electrons, respectively. Similarly, BETAN.PFMOB and BETAP.PFMOB are the electron and hole Poole-Frenkel factors respectively. Poole-Frenkel model cause convergence issues since it is strongly dependent on electric field. For improvement in stability, Eqs. (13) and (14) are used,

$$\mu_p(E) = \frac{1}{\frac{1}{\mu_{p_{\mathrm{PF}}}(E)} + \frac{1}{\mu_{p_{\mathrm{lim}}}(E)}}, \tag{13}$$

$$\mu_n(E) = \frac{1}{\frac{1}{\mu_{n_{\mathrm{PF}}}(E)} + \frac{1}{\mu_{n_{\mathrm{lim}}}(E)}}, \tag{14}$$

where $\mu_n(E)$ is the electron mobility and $\mu_p(E)$ is hole mobility and $\mu_{p_{\mathrm{lim}}}(E)$ and $\mu_{n_{\mathrm{lim}}}(E)$ are the limiting mobility for the both thermal velocities. PF here denotes the Poole-Frenkel factors due to the use of Poole-Frenkel mobility model.

4 Results and discussion

To increase the current density, HAT-CN layer is inserted between anode (ITO) and Meo-Spiro TPD layers. It is clear from Fig. 3 that inserting HAT-CN layer in between the two mentioned layers result in drastic increase in current density with respect to applied voltage. This is due to the fact that HAT-CN molecule increases the efficiency (hole transport) of p-type organic materials. Reason for this is the presence of six strong electron affinity acetonitrile groups in the HAT-CN material. These acetonitrile groups contribute in the deeply present LUMO energy levels [15].

Similarly, *I-V* characteristics with and without HAT-CN layer inserted is shown in Fig. 4. It is clear from Fig. 4 that same curve criterion is followed for the *I-V* characteristics also. That is, there is large increase in anode current with

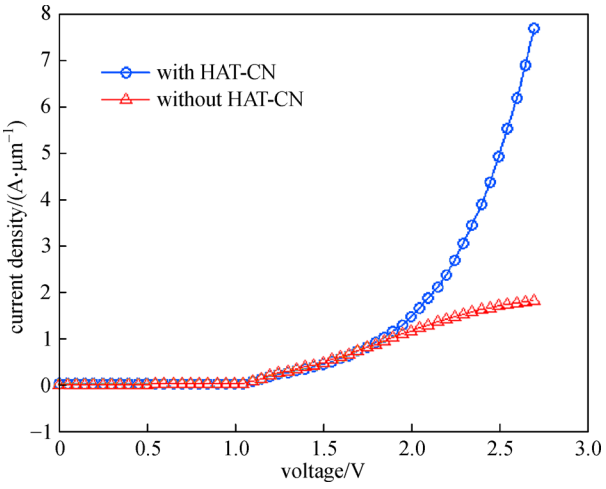

Fig. 3 Current density versus voltage for device with and without HAT-CN

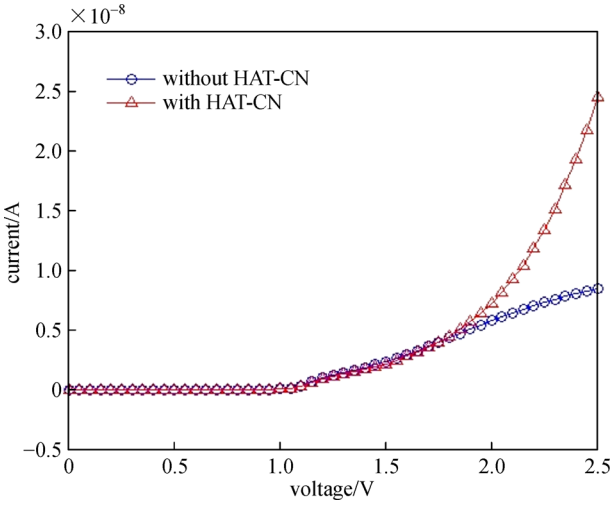

Fig. 4 *I-V* characteristics comparison with and without HAT-CN

Table 1 Current and current density comparison with and without HAT-CN layer

S. No.	parameter	without HAT-CN	withHAT-CN
1	current	0.01 μA	5.79 μA
2	current density	2.0 A/μm	1160 A/μm

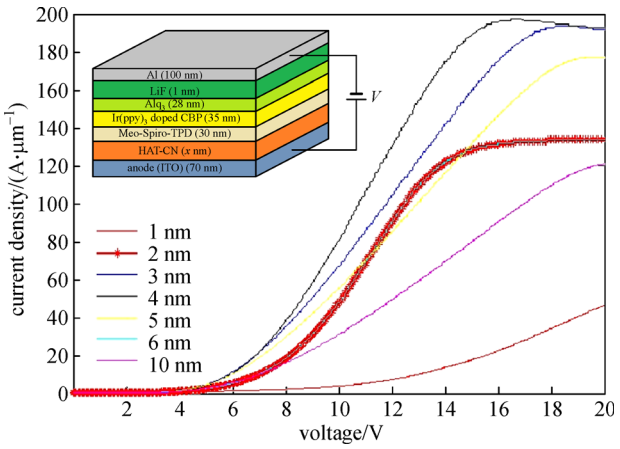

Fig. 5 Current density versus voltage for different HAT-CN thickness

respect to applied voltage on the addition of HAT-CN layer.

Table 1 shows the values of current and current density without HAT-CN layer and with the insertion of HAT-CN layer.

Also, different material layer thicknesses have been optimized in order to increase the current density with respect to voltage and hence to enhance the efficiency. Figure 5 shows the optimization of HAT-CN layer for better current density value. Here structure shown in the inset of Fig. 5 is simulated for different HAT-CN thickness (1, 2, 3, 4, 5, 6 and 10 nm) and it is found that maximum current density is approached at 4 nm HAT-CN thickness.

Figure 6 shows CBP layer thickness optimization for the best value of current density with respect to applied voltage. It shows that current density is maximum for a CBP layer thickness of 25 nm. Inset of Fig. 6 shows the structure which is simulated for x (nm) thickness of $Ir(ppy)_3$ doped CBP where x = 20, 24, 25, 30 and 40 nm.

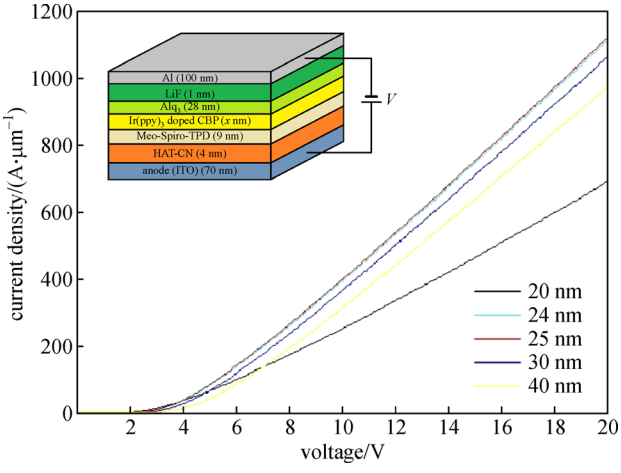

Fig. 6 Current density versus voltage for different CBP doped with $Ir(ppy)_3$ thickness

Thickness of EML plays a significant role in the study of device performance. It was reported in Ref. [22] that when we reduce the thickness of EML, due to the diffusion of recombination zone, efficiency is reduced (causes blue shift in electroluminescence (EL)) and increase in thickness causes red shift in EL. External quantum efficiency of OLEDs drops at higher luminance and this is called as "efficiency roll-off"(ERO). It occurs due to the lack of exciton confinement in EML. Doping of CBP with $Ir(ppy)_3$ results in reduction of efficiency roll-off [23].

Similarly, optimization curves for Meo-Spiro TPD and Alq_3 are shown for the best possible values of current density with respect to voltage variation. It is found that Meo-Spiro TPD is optimized at 9 nm layer thickness and Alq_3 is optimized for 22 nm thickness. Combining all these optimization results, best possible current density results for structures shown in the insets of respective figures have been find out. These are clear from Figs. 7 and 8.

Table 2 shows thickness versus current density comparison for different materials. From Table 2, considering the current density values at different thicknesses, it can be

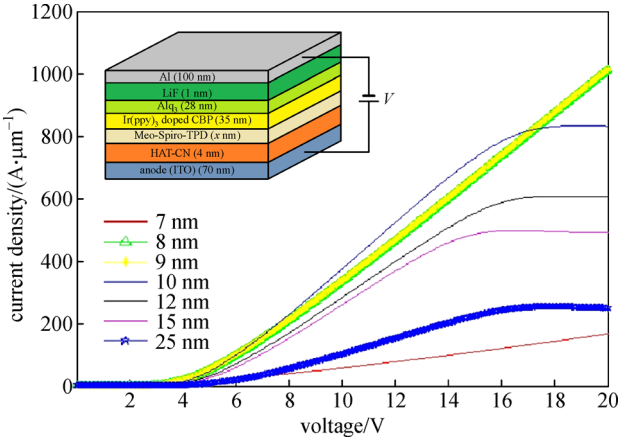

Fig. 7 Current density versus voltage for different Meo-Spiro TPD thickness

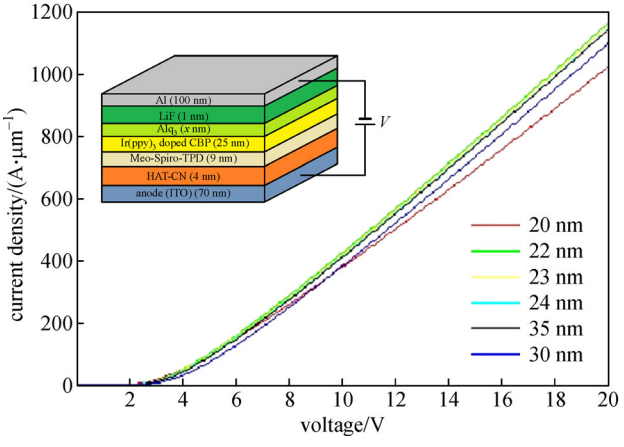

Fig. 8 Current density versus voltage for different Alq_3 thickness

Table 2 Current density with respect to variation in layer thickness for different materials

S. No.	material	thickness/nm	current density/(A·μm^{-1})
1	HAT-CN	1	46.5
		3	191
		4	198
		6	162
		10	121
2	Ir(ppy)$_3$ doped CBP	20	688
		24	1120
		25	1110
		30	1066
		40	968
3	Meo-Spiro-TPD	7	165
		9	1010
		10	832
		15	497
		25	253
4	Alq$_3$	20	1020
		22	1170
		24	1150
		25	1140
		30	1090

concluded that for Alq$_3$ material, at a thickness of 22 nm, the maximum current density value is approxomately 1.2 A/cm.

Figure 9 shows the recombination curve with respect to applied voltage. This curve shows the effect of applied voltage on the recombination phenomena. These characteristics were accredited to the excited cavernous and shallow trap levels and the change of recombination zone. In Fig. 9, as the voltage increases, the recombination zone would be changed, which had further effects on the recombination efficiency. Here as the voltage increases, recombination and hence the recombination efficiency decreases. The reduced interfacial energy barrier enhances the hole current density at the anode/organic interface [12]. Furthermore, the electric field curve with respect to applied voltage along the EML, as shown in Fig. 10, increased steadily from ITO/EML interface also influenced the recombination versus voltage at the EML [6].

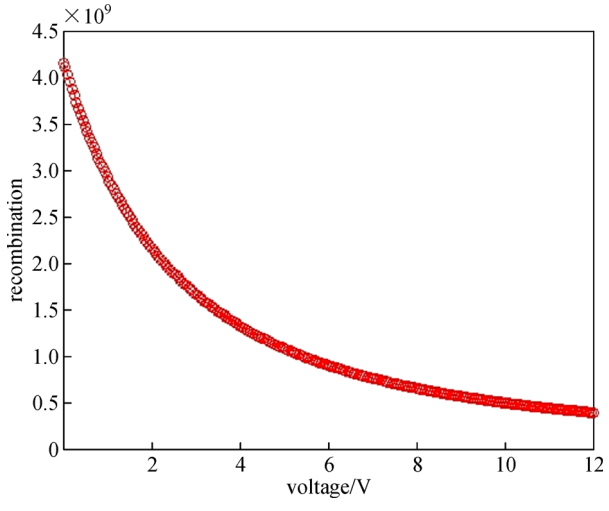

Fig. 9 Recombination versus applied voltage for the OLED structure

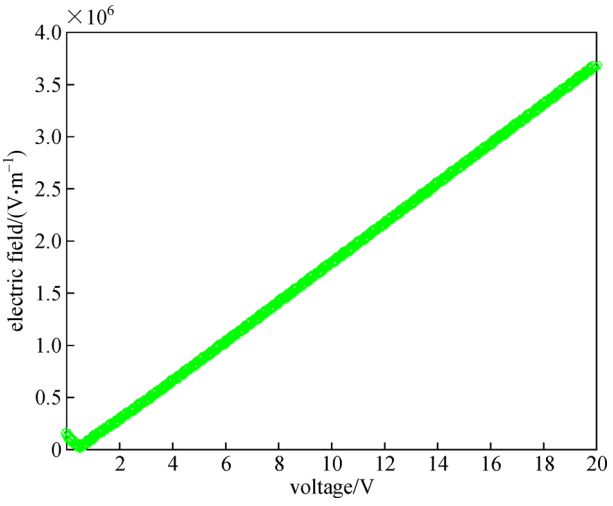

Fig. 10 Electric field versus applied voltage for device

Figure 10 shows the linear increase in electric field with respect to applied voltage. This shows that organic materials used in the device structure are electric field dependent.

Figure 11 shows the almost linear dependence of $\sqrt{F}$ on natural log of current density, which confirms the thermionic injection of charge carriers in the device.

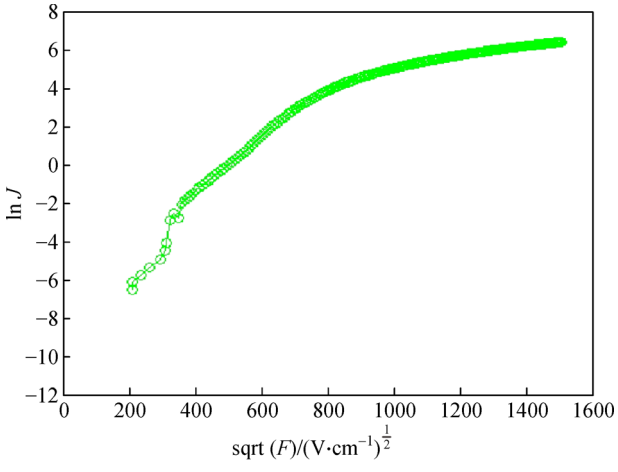

Fig. 11 $\sqrt{F}$ versus ln (current density) curve

Figure 10 signifies for the values of electric field to be used for the calculation in Fig. 11.

5 Conclusion

To sum up, we have investigated the outcome of inserting HAT-CN layer in the stacked nano-structured organic light emitting diode at the organic/metal interface. Adding HAT-CN layer in the OLED structure results in drastic boost in current density and hence the efficiency. This is due to the creation of dipoles at the interface. The present paper is based on the optimization of organic layers in order to maximize the current density and efficiency. Charge injection from the electrodes is dependent on the Richardson thermionic emission equations which are mentioned in the above sections. Also, it has been observed that enhanced current density is due to the insertion of HAT-CN which lowered the barrier height at the interface and hence increases the injection efficiency.

Acknowledgements Authors wish to express their gratitude to Amity University, Noida for supporting this simulation work.

References

1. Joo C W, Lee K, Lee J, Cho H, Shin J W, Cho N S, Moon J. Optical and structural approaches for improved luminance distribution and enhanced efficiency of organic light emitting diodes. Journal of Luminescence, 2017, 187: 433–440
2. Rajan G, Yadav V, Manzhi P, Chauhan G, Suman C K, Srivastava R, Sinha O P. Study of injection and transport properties of metal/organic interface using HAT-CN molecules as hole injection layer. Vacuum, 2017, 146: 530–536
3. Juhasz P, Nevrela J, Micjan M, Novota M, Uhrik J, Stuchlikova L, Jakabovic J, Harmatha L, Weis M. Charge injection and transport properties of an organic light-emitting diode. Beilstein Journal of Nanotechnology, 2016, 7: 47–52
4. Kung T J, Huang J Y, Huang J J, Tseng S H, Leung M K, Chiu T L, Lee J H, Wu Y R. Modeling of carrier transport in organic light emitting diode with random dopant effects by two-dimensional simulation. Optics Express, 2017, 25(21): 25492–25503
5. Méndez-Pinzón H A, Pardo-Pardo D R, Cuéllar-Alvarado J P, Salcedo-Reyes J C, Vera R, Páez-Sierra B A. Analysis of the current-voltage characteristics of polymer-based organic light-emitting diodes (OLEDs) deposited by spin coating. Javeriana, 2010, 15(1): 68–76
6. Chowdhury R, Haq M R, Chowdhury M S U, Afrose S, Paul S. Effect of higher carrier injection rate on charge transport and recombination in mixed-host organic light emitting diode. In: Proceedings of International Conference on Innovations in Science, Engineering and Technology (ICISET), IEEE, 2016
7. Fišerová E, Kubala M. Mean fluorescence lifetime and its error. Journal of Luminescence, 2012, 132(8): 2059–2064
8. Lysenko I A, Patrashanu L A, Zyko D D. Organic light emitting diode simulation using Silvaco TCAD tools. In: Proceedings of International Siberian Conference on Control and Communications (SIBCON), 2016
9. Atlas User's Manual. Device Simulation Software. Santa Clara, 2013, (408): 567–1000
10. Tobat P, Saragi I, Spehr T, Siebert A, Lieker T F, Salbeck J. Spiro compounds for organic optoelectronics. Chemical Reviews, 2007, 107(4): 1011–1065
11. Grover R, Srivastava R, Dagar J, Kamalasanan M N, Mehta D S. Interface modified thermally stable hole transporting layer for efficient organic light emitting diodes. Journal of Applied Physics, 2014, 116(6): 063102
12. Xu X M, Peng J C, Li H J, Qu S, Zhao C J. Effect of temperature and applied voltage on the recombination efficiency in double layer organic light emitting diodes. Spectroscopy and Spectral Analysis, 2004, 24(1): 12–14 (in Chinese)
13. Wang B, Zhang L, Hu Y, Shi X B, Wang Z K, Liao L S. Doped hole injection bilayer for solution processable blue phosphorescent organic light-emitting diodes. Journal of Materials Chemistry C, Materials for Optical and Electronic Devices, 2016, 4(27): 6570–6574
14. Tang X, Ding L, Sun Y Q, Xie Y M, Deng Y L, Wang Z K, Liao L S. Inverted and large flexible organic light-emitting diodes with low operating voltage. Journal of Materials Chemistry C, Materials for Optical and Electronic Devices, 2015, 3(48): 12399–12402
15. Zhang L, Zu F S, Deng Y L, Igbari F, Wang Z K, Liao L S. Origin of enhanced hole injection in organic light-emitting diodes with an electron-acceptor doping layer: p-type doping or interfacial diffusion? ACS applied materials & interfaces, 2015, 7(22): 11965–11971
16. Ding L, Tang X, Xu M F, Shi X B, Wang Z K, Liao L S. Lithium hydride doped intermediate connector for high-efficiency and long-term stable tandem organic light-emitting diodes. ACS Applied Materials & Interfaces, 2014, 6(20): 18228–18232
17. Lee W H, Jesuraj J, Song M, Hafeez H. Improvement of charge balance, recombination zone confinement, and low efficiency roll-off in green phosphorescent OLEDs by altering electron transport layer thickness. Material Research Express, 2018, 5: 076201
18. Salehi A, Ho S, Chen Y, Peng C, Yersin H, So F. Highly efficient organic light-emitting diode using a low refractive index electron transport layer. Advanced Optical Materials, 2017, 5: 197–204
19. Murawski C, Liehm P, Leo K, Gather M C. Influence of cavity thickness and emitter orientation on the efficiency roll-off of phosphorescent organic light-emitting diodes. Advanced Functional Materials, 2014, 24(8): 1117–1124
20. Terence D. Quantum simulation of thermionic emission from diamond films. Journal of Vacuum Science & Technology B Microelectronics and Nanometer Structures, 2013, 31(2): 021401
21. Fishchuk I I, Kadashchuk A K, Vakhnin A, Korosko Yu, Bässler H, Souharce B, Scherf U. Transition from trap-controlled to trap-to-trap hopping transport in disordered organic semiconductors. Physical Review B: Condensed Matter and Materials Physics, 2006, 73(11): 115210–1155221
22. Jesuraj P J, Hafeez H, Kim D H, Lee J C, Lee W H, Choi D K, Kim C H, Song M, Kim C S, Ryu S Y. Recombination zone control without sensing layer and the exciton confinement in green

phosphorescent OLEDs by excluding interface energy transfer. Journal of Physical Chemistry C, 2018, 122(5): 2951–2958

23. Gao Z, Wang F, Guo K, Wang H, Wei B, Xu B. Carrier transfer and luminescence characteristics of concentration-dependent phosphorescent Ir(ppy)3 doped CBP film. Optics & Laser Technology, 2014, 56: 20–24

Neha Jain received her M.Tech degree from Kurukshetra University, Kurukshetra in 2012. Now, she is a PhD candidate in Amity University, Noida in Department of Electronics and communication engineering under Amity School of Engineering and Technology. Her main research is focussed on theoretical simulation and fabrication of nano-structured devices for the electrical and optical properties and optoelectronic applications.

E-mail: aceneha@gmail.com

Prof. O. P. Sinha received his B.Sc. Hons and M.Sc. degrees in Physics from Magadh University, Bodh-Gaya in 1991 and 1993 respectively. He has done his PhD from Banaras Hindu University, Varanasi in 2001. He is working as Professor and Dy. Director in Amity Institute Of Nano-Technology, Amity University, Uttar Pradesh, Noida, India. He worked as Post Doctoral Researcher at Advanced Surface Technology Research Laboratory (ASTRaL) Lappeenranta University of Technology; Mikkeli, Finland and Guest scientist at Institute of Ion Beam Physics and Materials Research,Forschungszentrum Dresden-Rossendorf, Dresden, Germanyin 2009. He was a Marie Curie Fellow (Senior Visiting Research Fellow) at Centre for Nanometer-scale Science and Advanced Materials (NANOSAM), Department of Physics of Nanostructures and Nanotechnology, Institute of Physics, Jagiellonian University, Krakow, Poland in 2007 – 2008. His main research work is on semiconductor nanostructures, 2D nano-materials for optoelectronic applications.

E-mail: opsinha@amity.edu

Prof. Sujata Pandey received her Master's degree in Electronics (VLSI) and Ph.D. degree in Electronics from University of Delhi. Presently she is working as Professor at Amity University Uttar Pradesh. She has over 200 research publications in reputed international journals/conferences. Her areas of research are microelectronics, analog/digital VLSI design, and energy harvesting. She is member of IEEE, USA, member of Electron Device Society, IET UK, founder member of VLSI and Semiconductor Society of India, ISTE and life member of Indian Science Congress.

E-mail: spandey@amity.edu